Clim. Past Discuss., 8, 1275–1300, 2012
www.clim-past-discuss.net/8/1275/2012/
doi:10.5194/cpd-8-1275-2012

Climate of the Past Discussions

Isotopic and lithologic variations of one precisely dated stalagmite across the Medieval/LIA period from Heilong Cave, Central China

Y. F. Cui[1], Y. J. Wang[1], H. Cheng[2,3], K. Zhao[1], and X. G. Kong[1]

[1]College of Geography Science, Nanjing Normal University, Nanjing, 210097, China
[2]Institute of Global Environmental Change, Xi'an Jiaotong University, Xi'an, 710049, China
[3]Department of Geology and Geophysics, University of Minnesota, Minneapolis, Minnesota, 55455, USA

Received: 28 March 2012 – Accepted: 4 April 2012 – Published: 17 April 2012

Correspondence to: Y. J. Wang (yjwang@njnu.edu.cn)

Published by Copernicus Publications on behalf of the European Geosciences Union.

Abstract

Lithologic and isotopic changes of one stalagmite (224 mm in length) from Heilong Cave, Central China, are here investigated in order to explore multiple speleothem proxies of monsoon climate. High uranium concentrations (6–10 ppm) ensure Th-230 dates precisely and resultant chronology ranges from ~790 AD to 1780 across the Medieval Warm Period (MWP) to Little Ice Age (LIA). Annually resolved oxygen and carbon isotopic data, gray level and elemental Sr are highly related to macroscopic lithologic changes. A lamination sequence is composed of alternations of white-porous and dark-compact calcite clearly discerned on the polished surface. The dark-compact laminae have low values of gray level, high Sr and $\delta^{13}C$ values, indicating periods of low growth rate under dry climate conditions, and vise versa for the white-porous laminae. This suggests that changes in hydrology, matter input of drip water and crystallization process were controlled by cave environments and climates. The alternation of dry and wet periods with a significant periodicity of ~90 yr, as indicated by spectral analysis of the multiple proxies, is further supported by a reconstructed precipitation index by historical documents and instrumental data extending back to 1470 AD. A strong coherence between monsoon proxy of calcite $\delta^{18}O$ and the other proxies was observed during the LIA but not during the MWP. This is likely due to changes in atmospheric circulation pattern at the boundary of MWP/LIA. When the Intertropical Convergence Zone shifted southward during the LIA, summer monsoon precipitation at the cave site was probably dominated by the Mei-Yu, resulting in water vapor mainly originated from adjacent oceanic sources.

1 Introduction

The Medieval Warm Period (MWP) and Little Ice Age (LIA) are intensively concerned climate episodes during the last two millennia (Bradley and Jones, 1992; Esper et al., 2002; Bradley et al., 2003). Numerous studies have investigated the spatial patterns

CPD
8, 1275–1300, 2012

and causal factors underlying them (Mann et al., 2009; Kaufman et al., 2009). The centennial-scale oscillation has involved a significant perturbation in tropical ocean temperatures as well as monsoon rainfall (Newton et al., 2006). The episodic and widespread Asian monsoon droughts during the LIA were thought to have played a major role in significantly changing regional society at that time (Cook et al., 2010; Buckley et al., 2010). However, it still remains unclear about the spatiotemporal pattern of the Asian monsoon rainfall and its forcing mechanism partly due to inadequate high-resolution and long-term climate observations.

Considerable progress in reconstructing Asian monsoon (AM) climate over the past millennia has been made in using climate "proxy" data, such as ice cores (Thompson et al., 2000; Yang et al., 2007), tree rings (Cook et al., 2010; Buckley et al., 2010), lake sediments (Yancheva et al., 2007; Chu et al., 2009) and historical documents (Zheng et al., 2006; Tan et al., 2008). Speleothems are important terrestrial archives in recording AM climate for the past two millennia (Tan et al., 2003, 2006; Sinha et al., 2007, 2011; Zhang et al., 2008), as they have a great potential in dating, resolution and distribution (McDermott et al., 2004; Fairchild et al., 2006). The stalagmite $\delta^{18}O$ signal has been the extensively and successfully applied monsoon proxy, such as records from India and the Middle East (Sinha et al., 2011; Fleitmann et al., 2004, 2007) and data from China (Zhang et al., 2008; Wang et al., 2005; Hu et al., 2008). All of these $\delta^{18}O$ records indicated an accordant monsoon evolution trend: an increase in MWP and decrease in LIA. In East China, however, an integrated analysis of instrumental and historical records suggested a complex spatial rainfall pattern for the MWP and LIA, probably due to different responses of local rainfall to changes in regional monsoon intensity (Zhang et al., 2010). It is therefore necessary to utilize multiple proxies in stalagmite to investigate cave temperature, rainfall and vegetation response, in order to test a relationship of local climate changes and regional monsoon changes. Measurable parameters indicative of local environment changes include carbon isotope ratio, inter-annual thickness of growth laminae, trace-element ratios, organic acid contents and the nature of trapped pollen grains (Fairchild et al., 2006).

CPD
8, 1275–1300, 2012

Here, we explore multiple parameters from one stalagmite from Heilong Cave, Central China to investigate the climatic and environmental changes during the MWP and LIA. The trace element and stable isotope variations have largely been accounted for progressive CO_2 degassing and calcite precipitation from an initially saturated solution (Johnson et al., 2006), and may be related to seasonal rainfall changes. Additionally, the lithological changes, as alternations of annually deposited white-porous and dark-compact laminae, have been explained by the highly seasonal variations of the water excess (Genty and Quinif, 1996). Two issues are concerned: (1) climatic relationship between macroscopic lithologic changes and multi-proxy sequences; (2) shifts of monsoon circulation mode across the Medieval/LIA period, inferred from multiple parameters.

2 Material and methods

Heilong Cave (31°40′ N, 110°26′ E, elevation 1220 m) is located on the north slope of Mountain Shennongjia, over the middle reaches of Yangtze River Valley, Central China. Densely forested vegetation at the cave and surrounding area consists primarily of temperate deciduous broad-leaved plants. The cave was formed in Permian limestone, and is approximately 600 m in length with a narrow entrance. The relative humidity inside is close to 100 %. Regional climate is dominated by the East Asian monsoons (EAM) (Fig. 1). Mean annual precipitation between 1000 mm and 1500 mm shows a significant seasonal variation. During boreal summer (June to August), the inflow of warm/humid air from equatorial Pacific penetrates into the Mt. Shennongjia, delivering more than 50 % of total annual precipitation. Much less precipitation (~5 %) occurs during the winter monsoon months (December to February). Heilong Cave, together with previously reported Sanbao (close to Heilong) (Wang et al., 2008) and Hulu Cave (~800 km E) (Wang et al., 2001)are located within the Maiyu frontal zone of the EAM system, along which summer monsoon rains burst simultaneously in mid-June. Instrumental data of the past 30 yr (1971–2000) in China display that Mei-yu rainfalls (from 17 June to 8 July)

CPD
8, 1275–1300, 2012

are mainly distributed over the mid-low Yangtze River Valley, with concentrated and intensive rainfall of 200–300 mm, accounting for about 45 % of total summer (June, July and August) rainfall amount (Ding and Chan, 2005; Ding et al.,2007). Mean annual surface temperature is about 8–13 °C, reaching a maximum in July (mean ~22 °C) and a minimum in January (~1 °C). Drip rate of seepage water inside the cave increases during the rainy seasons, and decreases dramatically during the dry seasons, following the seasonal cycle of local precipitation.

The columnar-shaped stalagmite BD is 224 mm in length, and its diameter ranges between 27 and 88 mm. The sample was halved along the growth axis and polished, showing alternations of white-porous and dark-compact laminations (Fig. 2a). Fairly short sections present visible annual layers, identifiable with the naked eye (Fig. 2b,c), despite that the annual laminations do not persist throughout the whole sequence.

Eleven sub-samples were collected for U-Th dating. Approximately 100 mg samples of powder were extracted by milling along growth horizons with a hand-held carbide dental drill. Procedures for chemical separation and purification of uranium and thorium are similar to those described in Edwards et al. (1987) and Cheng et al. (2000). Measurements were performed on a Finnigan Element inductively coupled plasma mass spectrometer (ICP-MS), equipped with a double-focusing sector magnet and energy filter in reversed Nier-Johnson geometry and a MasCom multiplier, following procedures described in Shen et al. (2002). This work was performed at the Minnesota Isotope Laboratory, University of Minnesota.

A total of 1103 sub-samples were collected on average of every 0.2 mm along the central growth axis for isotopic analysis by knife shaving. The measurement was performed on a Finnigan-MAT 253 mass spectrometer fitted with a Kiel Carbonate Device at the College of Geography Science, Nanjing Normal University. Stable isotope measurements are similar to those described in Dykoski et al. (2005), with results that were reported relative to Vienna PeeDee Belemnite (VPDB) and with standardization determined relative to NBS19. Precision of δ^{18}O values is 0.06 ‰, at the 1-sigma level.

CPD
8, 1275–1300, 2012

A proxy of gray level was measured on a scanned picture of the polished surface taken with a high-resolution scanner. The data were obtained using ENVI software with a 4 mm wide traverse along the central growth axis. Gray levels vary between 20 and 250 with a mean of 99. The trace element analyses were produced by the Avaatech XRF Core Scanner (X-ray fluorescence spectrometry), which is equipped with a variable optical system that enables any resolution between 10 and 0.1 mm (here, 0.5 mm resolution). This work was performed at the Surficial Geochemistry Laboratory, Nanjing University.

3 Results

3.1 Chronology

Eleven ^{230}Th dates are used to develop chronology for stalagmite BD (Fig. 3), with typical errors (2σ) of about 0.5 % (Table 1). The resultant dates are in stratigraphic order and range from 860 AD to 1780 AD, with most of the deposition across the MWP and LIA. Errors are small, from ±3 to ±20 yr, due to high uranium concentrations (from 6 to 9.6 ppm). Over the dated interval, the average growth rate is 22.4 mm/100 yr. An age model of stalagmite is based on linear interpolation between ^{230}Th dates. The average sampling interval for the stable isotope analyses is ~0.8 yr.

3.2 Proxy sequences

Equilibrium calcite precipitation is important in order to interpret calcite δ^{18}O in terms of climate. A "Hendy Test" (Hendy, 1971), performed on six individual growth laminae, shows that δ^{18}O variations along the same layer are less than 0.3 ‰ (Fig. 4a) and correlations between carbon and oxygen are statistically insignificant (Fig. 4b). These results indicate that the stalagmite calcite was deposited in isotopic equilibrium and the δ^{18}O signal is primarily of climate origin. δ^{18}O values range from −9.2 ‰ to −7.4 ‰,

CPD
8, 1275–1300, 2012

with an overall mean of −8.3‰ (Fig. 5). The $\delta^{18}O$ profile exhibits significant fluctuations, and no long-term trend is observed throughout the whole profile. The amplitude seems larger during the interval of 0 ~ 73 mm (mainly covering the LIA, approximately 1.3‰) than the other part. Previous studies suggested that shifts in stalagmite $\delta^{18}O$ largely reflect changes in $\delta^{18}O$ values of meteoric precipitation at Hulu and Sanbao Caves. These shifts, in turn, likely relate to changes in summer monsoon intensity (Cheng et al., 2006, 2009; Wang et al., 2001, 2008). The isotopic composition of modern precipitation from the nearest meteorological station (Wuhan, 30.62° N, 114.13° E) exhibits a distinct seasonal signal (Araguás-Araguás et al., 1998). Weighted mean annual $\delta^{18}O$ value for the period from 1988–1996 was −7.0‰, with more negative values in summer months (average −9.5‰, SMOW) and more positive $\delta^{18}O$ in winter months (average −4.5‰, SMOW). More negative $\delta^{18}O$ values are consistent with a greater contribution of summer rainfall, associated with strong summer monsoon circulation. Therefore, we interpret the $\delta^{18}O$ record from Heilong Cave in the same manner as the Sanbao and Hulu records.

$\delta^{13}C$ values range from −14.9‰ to −10.5‰, with an average of −12.4‰ (Fig. 5). The $\delta^{13}C$ curve shows a striking similarity to the $\delta^{18}O$ during the interval of 0 ~ 73 mm (corresponding to the LIA) with five peaks and five troughs and notable differences in the rest (the MWP). The amplitude seems smaller in the LIA (~2.5‰) in contrast to the MWP (~3.74‰, Fig. 6a). Variations of $\delta^{13}C$ depend upon type of vegetation (C3 or C4), drip rate of water, bedrock dissolution rate and seasonal variations in the soil CO_2 in a complex fashion (Genty et al., 2001; McDermott et al., 2004; Fairchild et al., 2006). Therefore, stalagmite $\delta^{13}C$ records can be used as an indicator of local environmental changes.

Elemental Sr profile is illustrated in Fig. 5. The variations in the bulk Sr content generally range from 53 counts per second (cps) to 145 cps, with an average of 103 cps. Each measurement number has a spatial resolution of 0.5 mm distance. The Sr profile exhibits significant fluctuations and no long-term trend is observed throughout the whole profile. Since overlying limestone typically releases a significant amount of Sr,

CPD
8, 1275–1300, 2012

transported downward by the seepage water, the Sr in speleothems is expected to be derived mainly from the overlying limestone. Changes in the Sr content of a stalagmite can be controlled by dissolution-precipitation processes in the unsaturated zone, due to differences in water residence time (Roberts et al., 1998; Bar-Matthews et al., 1999; Fairchild et al., 2000). Thus, Sr content in stalagmite can be used as an indicator of drip rate, and then likely reflects dry/wet conditions at the cave site.

4 Discussions

4.1 Link between climatic and lithological changes

As mentioned before, sample BD exhibits alternations of white-porous and dark-compact calcite. In Fig. 5, gray level directly reflects the macroscopic lithological changes, with high values of gray level, corresponding to white-porous phases, whereas low values to dark-compact phases. Comparison between $\delta^{13}C$ and gray level shows a good relationship, with negative and positive excursions of $\delta^{13}C$ values, corresponding to high (white-porous laminae) and low (dark-compact laminae) values of gray level, respectively (Fig. 5). The Sr profile has a substantial similarity to gray level and $\delta^{13}C$ curves. High Sr intensities are closely associated with the dark-compact laminae, while low to white-porous laminae (Fig. 5). However, there are some discrepancies among them, likely due to analysis errors from pore spaces on the polished surface (Fig. 2a) and different analysis tracks among them (Fig. 5).

As shown in Fig. 3, changes in growth rate can be divided into two distinct intervals. The first phase (0 ~ 75 mm from the top, spanning the LIA), containing more dark-compact laminae, shows much lower growth rate (~15 mm/100 yr) than that (~29 mm/100 yr) in the second phase (75 ~ 220 mm, in MWP), encompassing more white-porous laminae (Fig. 5). The lowest growth rate (~10 mm/100 yr) of the sample falls within the first part, from 29 ~ 58 mm depth, signaling the summit of LIA. The maximum growth rate interval (~63 mm/100 yr), between 148 ~ 192 mm depths, was dated

CPD
8, 1275–1300, 2012

at the beginning of MWP. The changes in growth rate deduced from ^{230}Th dates can be further evaluated by the sparse and faint annual-bands. In the white-porous laminae, thickness of annual visible bands varies approximately from 300 ~ 900 µm, averaging at ~570 µm (Fig. 2b). The white, dark paired laminae resemble the white-dark couplets described in a stalagmite from Heshang Cave (close to Heilong Cave, Johnson et al., 2006), probably due to a similar climate that has a strong seasonality. In the dark-compact laminae, annual bands vary approximately from 45 ~ 120 µm, averaging at ~85 µm (Fig. 2c), close to those of annual microbanding in stalagmites from North China (Tan et al., 2006, Hou et al., 2002). These observations suggest that changes in growth rate are consistent with the macroscopic lithological changes, with high growth rate corresponding to white-porous laminae and low to dark-compact laminae.

Genty and Quinif (1996) have proposed that the annual variations of drip rate and super-saturation, due to seasonality in the seepage water, may produce some degree of crystalline coalescence, thus forming compact versus porous layers. In the same manner, the seasonal variation of compact versus porous layers could occur at a decadal-centennial timescale. In our study region where vegetation type is predominantly C3 forest, the influence of vegetation on stalagmite δ^{13}C primarily reflects changes in the density of vegetative cover and biomass (Baldini et al., 2005). In dry years, limited vegetation growth and soil CO_2 production could lead to less contribution of biogenic CO_2 dissolving in the seepage water and high speleothem δ^{13}C values, and vice versa. Additionally, reduced/increased drip rates under dry/wet conditions could result in high/low speleothem δ^{13}C values, owing to more/less time for CO_2 degassing (Bar-Matthews et al., 1996; Mühlinghaus et al., 2007; Romanov et al., 2008). Therefore, a good relationship between δ^{13}C, Sr and visible lithological changes in sample BD suggests that dark-compact structures were formed under dry conditions (low drip rate), and white-porous laminae were formed under wet conditions (high drip rate).

CPD
8, 1275–1300, 2012

4.2 Monsoon changes across the MWP/LIA

The intra-seasonal monsoon variability is dominated by the "active" and "break" spells – two distinct oscillatory modes of monsoon that have radically different synoptic scale circulation and precipitation patterns (Annamalai and Slingo, 2001; Rajeevan et al., 2010). The seasonal cycle is a plausible analog for decadal-centennial scale strong/weak monsoon alternations. Lines of evidence suggest that stronger monsoons, related to northward shifts of Intertropical Convergence Zone (ITCZ), may be associated with a protracted phase of the "active-dominated" mode during the MWP, and vice versa for the LIA (review in Sinha et al., 2011). As mentioned before, the relationship of the $\delta^{18}O$ and $\delta^{13}C$ series is strong during LIA, with a Pearson correlation coefficient of 0.46 ($n = 407$, $p < 0.001$). The $\delta^{18}O$ profile also bears a remarkable resemblance to gray level and Sr intensities during that period (Fig. 6b). In contrast, notable differences occur between the $\delta^{18}O$ and the other proxies during MWP (790 ~ 1320 AD), with a low Pearson correlation coefficient of ~0.18 ($\delta^{18}O$ vs. $\delta^{13}C$) (Figs. 5 and 6a). This suggests that changes in large-scale monsoon circulation may be responsible for the coupling of the regional $\delta^{18}O$ signal and the local environmental proxies since the beginning of LIA.

The Asian summer monsoon system consists mainly of the ITCZ (tropical monsoon trough) and Subtropical Convergence Zone (Mei-Yu front) (Tao and Chen, 1987). Meteorological studies have indicated an opposite relationship of intensities between ITCZ and Subtropical Convergence Zone (Zhang, 1998, 2001; Zhang and Tao, 1998). Previous studies from Asia (Yancheva et al., 2007; Sinha et al., 2011), Africa (Verschuren et al., 2000; Brown and Johnson, 2005), South America (Reuter et al., 2009; Bird et al., 2011) and Pacific Ocean (Oppo et al., 2009; Sachs et al., 2009) suggest that ITCZ has shifted substantially to its southernmost position during the LIA. Under the LIA colder climate condition, variability of Mei-Yu front, associated with the shift of the western North Pacific subtropical high in its intensity and location, appears to have played a major role in transporting moisture to the cave site in mid-low Yangtze River Valley.

CPD
8, 1275–1300, 2012

Therefore, the summer rainfall and its $\delta^{18}O$ at the cave site were probably controlled by a single moisture source linked to Mei-Yu, which originates from adjacent oceanic sources, with strong Mei-Yu intensity related to heavy rainfall and negative $\delta^{18}O$ values, and vice versa. Spectral analyses on the $\delta^{18}O$ and $\delta^{13}C$ records of stalagmite BD over the LIA show a significant peak at ~100 yr and ~90 yr, respectively (Fig. 7). These quasi-periodicities are consistent with the centennial cycle for the length of Mei-yu, reconstructed by historical documents and instrumental data extending back to 1736 AD (Ge et al., 2008) and the 90-yr oscillation exhibited in dry-wet indices of lower Yangtze River over the period 1470–1670 AD (Qian and Zhu, 2002). This suggests that the summer rainfall and its $\delta^{18}O$ at the cave site probably reflected the Mei-Yu intensity at LIA.

The Mei-Yu control of the cave environment during the LIA is further supported by a comparison of reconstructed summer (JJA) precipitation index by tree-ring and historical documents for North China (Yi et al., 2012) and our multi-proxy profiles. As shown in Fig. 6b, within dating uncertainties, each of the seven wet intervals at the cave site has its corresponding dry episode over North China, supporting the idea that changes in spatial rainfall patterns in China were controlled by the interaction between the tropic monsoon trough and the Mei-Yu front (Zhang and Tao, 1998; Ge et al., 2008), with weak (intense) tropic monsoon intensity corresponding to an intense (weak) Mei-Yu front, high (low) rainfall over the mid-low Yangtze River Valley, and low (high) precipitation over North China (Zhang, 2001; Qian et al., 2007). When ITCZ shifted northward during the MWP (Sachs et al., 2009; Sinha et al., 2011), water vapor for the summer rainfall over the mid-low Yangtze River Valley may come from a distant, tropical Indo-Pacific source and adjacent oceanic sources, leading to a complex relationship of rainfall $\delta^{18}O$ and its amount.

CPD
8, 1275–1300, 2012

5 Conclusions

Based on 11 precise ^{230}Th dates and measurements of physical, elemental and isotopic proxies of one stalagmite from Heilong Cave, Central China, we reconstructed annually-resolved monsoon climate changes from 790 to 1780 AD covering the MWP and LIA. Three conclusions can be drawn from multi-proxy investigations as follows:

1. Macroscopic lithologic changes, with alternations of white-porous and dark-compact laminae, are highly related to variations of multi-proxy profiles, which were mainly controlled by changes in cave environments and climates on decadal-centennial time scales. In general, dark-compact laminae have a low growth rate and gray level, high Sr intensities and δ^{13}C values, indicating periods under dry conditions, and vise versa for white-porous laminae. This suggests that macroscopic lithologic changes, analogous to seasonal fabric variations in annual laminae, can serve as an indicator of climatic or environmental changes.

2. High-resolution δ^{18}O, δ^{13}C, gray level and Sr profiles exhibit significant fluctuations without a long-term trend throughout the whole profiles. All records show low frequency oscillations in MWP and high frequency in LIA, with a significant periodicity of ~90 yr in LIA. The amplitude of δ^{13}C, gray level and Sr cycles is larger in MWP than that in LIA, but in an opposite sense to δ^{18}O. Contrasting with the MWP, δ^{18}O and δ^{13}C values are heavier and growth rate is lower during the LIA, indicating a relatively drier condition.

3. Relationship between the regional δ^{18}O signal and the local environmental proxies (δ^{13}C, gray level and Sr) switched to a coupled mode since LIA, likely due to a shift in atmospheric circulation patterns across the MWP/LIA. When ITCZ shifted southward during the LIA, water vapor and its δ^{18}O at the cave site were probably dominated by a single moisture source linked to the Mei-Yu, resulting in a simple relationship between rainfall δ^{18}O and its amount. Alternatively, when ITCZ shifted northward during the MWP, water vapor may come from various

CPD
8, 1275–1300, 2012

moisture sources, leading to an ambiguous relationship between rainfall $\delta^{18}O$ and its amount.

Acknowledgements. This work was supported by the National Nature Science Foundation of China (grant No. 2007105GZ10033), Basic Research Program of Jiangsu Province (grant No. BK2008025) and the CAS Strategic Priority Research Program (grant No. XDA05080503).

References

Annamalai, H. and Slingo, J. M.: Active/break cycles: Diagnosis of the intraseasonal variability of the Asian summer monsoon, Clim. Dynam., 18, 85–102, 2001.

Araguás-Araguás, L., Froehlich, K., and Rozanski, K.: Stable isotope composition of precipitation over Southeast Asia, J. Geophys Res., 103, 28721–28742, 1998.

Baldini, J., McDermott, F., Baker, A., Baldini, L., Mattey, D., and Railsback, B.: Biomass effects on stalagmite growth and isotope ratios: a 20th century analogue from Wiltshire, England, Earth Planet. Sc. Lett., 240, 486–494, 2005.

Bar-Matthews, M., Ayalon, A., Matthews, A., Sass, E., and Halicz, L.: Carbon and oxygen isotope study of the active water-carbonate system in a karstic Mediterranean Cave: implication for palaeoclimate research in semiarid regions, Geochim. Cosmochim. Acta, 60, 337–347, 1996.

Bar-Matthews, M., Ayalon, A., Kaufman, A., and Wasserburg, G. J.: The Eastern Mediterranean paleoclimate as a reflection of regional events: Soreq Cave, Israel, Earth Planet. Sc. Lett., 166, 85–95, 1999.

Bird, B. W., Abbott, M. B., Vuille, M., Rodbell, D. T., Stansell, N. D., and Rosenmeier, M. F.: A 2,300-yr-long annually resolved record of the South American summer monsoon from the Peruvian Andes, P. Natl. Acad. Sci. USA, 108, 8583–8588, 2011

Bradley, R. S. and Jones, P. D.: When was the "Little Ice Age"?, in: Proceedings of the International Symposium on the Little Ice Age climate, edited by: Mikami, T., Department of Geography, Tokyo Metropolitan University, 1–4, 1992.

Bradley, R. S., Hughes, M. K., and Diaz, H. F.: Climate in Medieval time, Science, 302, 404–405, 2003.

CPD

8, 1275–1300, 2012

Brown, E. T. and Johnson, T. C.: Coherence between tropical East African and South American records of the Little Ice Age, Geochem. Geophy. Geosy., 6, Q12005, doi:10.1029/2005GC000959, 2005.
Buckley, B. M., Anchukaitis, K. J., Penny, D., Fletcher, R., Cook, E. R., Sano, M., Nam, L. C., Wichienkeeo, A., Minh, T. T., and Hong, T. M.: Climate as a contributing factor in the demise of Angkor, Cambodia, P. Natl. Acad. Sci. USA, 107, 6748–6752, 2010.
Cheng, H., Edwards, R. L., Hoff, J., Gallup, C. D., Richards, D. A., and Asmerom, Y.: The half-lives of uranium-234 and thorium-230, Chem. Geol., 169, 17–33, 2000.
Cheng, H., Edwards, R. L., Wang, Y. J., Kong, X. G., Ming, Y. F., Gallup, C. D., Kelly, M. J., Wang, X. F., and Liu, W. G.: A penultimate glacial monsoon record from Hulu Cave and two-phase glacial terminations, Geology, 34, 217–220, 2006.
Cheng, H., Edwards, R. L., Broecker, W. S., Denton, G. H., Kong, X. G., Wang, Y. J., Zhang, R., and Wang, X. F.: Ice age terminations, Science, 326, 248–251, 2009.
Chu, G. Q., Sun, Q., Wang, X. H., Li, D., Rioual, P., Qiang, L., Han, J. T., and Liu, J. Q.: A 1600 yr multi-proxy record of paleoclimatic change from varved sediments in Lake Xiaolongwan, Northeastern China, J. Geophys Res., 114, D22108, doi:10.1029/2009JD012077, 2009.
Cook, E. R., Anchukaitis, K. J., Buckley, B. M., D'Arrigo, R. D., Jacoby, G. C., and Wright, W. E.: Asian monsoon failure and megadrought during the last millennium, Science, 328, 486–489, 2010.
Ding, Y. H. and Chan, J. C. L.: The East Asian summer monsoon: an overview, Meteorol. Atmos. Phys., 89, 117–142, 2005.
Ding, Y. H., Liu, J. J., Sun, Y., Liu, Y. J., He, J. H., and Song, Y. F.: A study of the synoptic-climatology of the Meiyu system in East Asia, Chin. J. Atmos. Sci., 31, 1082–1101, 2007.
Dykoski, C. A., Edwards, R. L., Cheng, H., Yuan, D. X., Cai, Y. J., Zhang, M. L., Lin, Y. S., Qing, J. M., An, Z. S., and Revenaugh, J.: A high-resolution, absolute-dated holocene and deglacial Asian monsoon record from Dongge Cave, China, Earth Planet. Sc. Lett., 233, 71–86, 2005.
Edwards, R. L., Cheng, J. H., and Wasserburg, G. J.: ^{238}U-^{234}U-^{230}Th-^{232}Th systematics and the precise measurement of time over the past 500 000 yr, Earth Planet. Sc. Lett., 81, 175–192, 1986/87.
Esper, J., Cook, E. R., and Schweingruber, F. H.: Low-frequency signals in long tree-ring chronologies for reconstructing past temperature variability, Science, 295, 2250–2253, 2002.

CPD
8, 1275–1300, 2012

Fairchild, I. J., Borsato, A., Tooth, A. F., Frisia, S., Hawkesworth, C. J., Huang, Y., McDermott, F., and Spiro, B.: Controls on trace element (Sr-Mg) compositions of carbonate cave waters: implications for speleothem climatic records, Chem. Geol., 166, 255–269, 2000.

Fairchild, I. J., Smith, C. L., Baker, A., Fuller, L., Spötl, C., Mattey, D., McDermott, F., and E. I. M. F.: Modification and preservation of environmental signals in speleothems, Earth-Sci. Rev., 75, 105–153, 2006.

Fleitmann, D., Burns, S. J., Neff, U., Mudelsee, M., Mangini, A., and Matter, A.: Palaeoclimatic interpretation of high-resolution oxygen isotope profiles derived from annually laminated speleothems from Southern Oman, Quaternary Sci. Rev., 23, 935–945, 2004.

Fleitmann, D., Burns, S. J., Mangini, A., Mudelsee, M., Kramers, J., Villa, I., Neff, U., Subbary, A.-A., Buettner, A., Hippler, D., and Matter, A.: Holocene ITCZ and Indian monsoon dynamics recorded in stalagmites from Oman and Yemen (Socotra), Quaternary Sci. Rev., 26, 170–188, 2007.

Ge, Q. S., Guo, X. F., Zheng, J. Y., and Hao, Z. X.: Meiyu in the middle and lower reaches of the Yangtze River since 1736, Chinese Sci. Bull., 53, 107–114, 2008.

Genty, D. and Quinif, Y.: Annually laminated sequences in the internal structure of some Belgian stalagmites-importance for paleoclimatology, J. Sediment. Res., 66, 275–288, 1996.

Genty, D., Baker, A., Massault, M., Procter, C., Gilmour, M., Pons-Banchu, E., and Hamelin, B.: Dead carbon in stalagmites: carbonate bedrock paleodissolution vs. ageing of soil organic matter. Implications for ^{13}C variations in speleothems, Geochim. Cosmochim. Acta, 65, 3443–3457, 2001.

Hendy, C. H.: The isotopic geochemistry of speleothems – I. The calculation of the effects of different modes of formation on the isotopic composition of speleothems and their applicability as palaeoc limatic indicators, Geochim. Cosmochim. Acta, 35, 801–824, 1971.

Hou, J. Z., Tan, M., and Liu, D. S.: Counting chronology and climate records with about 1000 annual layers of a Holocene stalagmite from the Water Cave in Liaoning Province, China, Sci. China Ser. D, 54, 385–391, 2002.

Hu, C. Y., Henderson, G. M., Huang, J., Xie, S. C., Sun, Y., and Johnson, K. R.: Quantification of Holocene Asian monsoon rainfall from spatially separated cave records, Earth Planet. Sc. Lett., 266, 221–232, 2008.

Johnson, K. R., Hu, C. Y., Belshaw, N. S., and Henderson, G. M.: Seasonal trace-element and stable-isotope variations in a Chinese speleothem: The potential for high-resolution paleomonsoon reconstruction, Earth Planet. Sc. Lett., 244, 394–407, 2006.

CPD
8, 1275–1300, 2012

Kaufman, D. S., Schneider, D. P., McKay, N. P., Ammann, C. M., Bradley, R. S., Briffa, K. R., Miller, G. H., Otto-Bliesner, B. L., Overpeck, J. T., Vinther, B. M., and Arctic Lakes 2k Project Members: Recent warming reverses long-term arctic cooling, Science, 325, 1236–1239, 2009.

Mann, M. E., Zhang, Z., Rutherford, S., Bradley, R. S., Hughes, M. K., Shindell, D., Ammann, C., Falugevi, G., and Ni, F.: Global signatures and dynamical origins of the "Little Ice Age" and "Medieval Climate Anomaly", Science, 326, 1256–1260, 2009.

McDermott, F.: Paleo-climate reconstruction from stable isotope variations in speleothems: a review, Quaternary Sci. Rev., 23, 901–918, 2004.

Mühlinghaus, C., Scholz, D., and Mangini, A.: Modelling stalagmite growth and δ^{13}C as a function of drip interval and temperature, Geochim. Cosmochim. Acta, 71, 2780–2790, 2007.

Newton, A., Thunell, R., and Stott, L. D.: Climate and hydrographic variability in the Indo-Pacific Warm Pool during the last millennium, Geophys. Res. Lett., 33, L19710, doi:10.1029/2006GL027234, 2006.

Oppo, D., Rosenthal, Y., and Linsley, B. K.: 2000-yr-long temperature and hydrology reconstructions from the Indo-Pacific warm pool, Nature, 460, 1113–1116, 2009.

Qian, W. H. and Zhu, Y. F.: Little ice age climate near Beijing, China, inferred from historical and stalagmite records, Quaternary Res., 57, 109–119, 2002.

Qian, W. H., Lin, X., Zhu, Y. F., Xu, Y., and Fu, J. L.: Climatic regime shift and decadal anomalous events in China, Climatic Change, 84, 167–189, 2007.

Rajeevan, M., Gadgil, S., and Bhate, J.: Active and break spells of the Indian summer monsoon, J. Earth Syst. Sci., 119, 229–247, 2010.

Reuter, J., Stott, L., Khider, D., Sinha, A., Cheng, H., and Edwards, R. L.: A new perspective on the hydroclimate variability in Northern South America during the Little Ice Age, Geophys. Res. Lett., 36, L21706, doi:10.1029/2009GL041051, 2009.

Roberts, M. S., Smart, P., and Baker, A.: Annual trace element variations in a Holocene speleothem, Earth Planet. Sc. Lett., 154, 237–246, 1998.

Romanov, D., Kaufmann, G., and Dreybrodt, W.: δ^{13}C profiles along growth layers of stalagmites: comparing theoretical and experimental results, Geochim. Cosmochim. Acta, 72, 438–448, 2008.

Sachs, J. P., Sachse, D., Smittenberg, R. H., Zhang, Z. H., Battisti, D. S., and Golubic, S.: Southward movement of the Pacific intertropical convergence zone AD 1400–1850, Nat. Geosci., 2, 519–525, 2009.

CPD
8, 1275–1300, 2012

Schulz, M. and Mudelsee, M.: REDFIT: Estimating red-noise spectra directly from unevenly spaced paleoclimatic time series, Comput. Geosci., 28, 421–426, 2002.
Shen, C. C., Edwards, R. L., Cheng, H., Dorale, J. A., Thomas, R. B., Moran, S. B., Weinstein, S. E., and Edmonds, H. N.: Uranium and thorium isotopic concentration measurements by magnetic sector inductively coupled plasma mass spectrometry, Chem. Geol., 185, 165–178, 2002.
Sinha, A., Cannariato, K. G., Stott, L. D., Cheng, H., Edwards, R. L., Yadava, M. G., Ramesh, R., and Singh, I. B.: A 900 yr (600 to 1500 AD) record of the Indian summer monsoon precipitation from the core monsoon zone of India, Geophys. Res. Lett., 34, L16707, doi:10.1029/2007GL030431, 2007.
Sinha, A., Stott, L., Berkelhammer, M., Cheng, H., Edwards, R. L., Buckley, B., Aldenderfer, M., and Mudelsee, M.: A global context for megadroughts in monsoon Asia during the past millennium, Quaternary Sci. Rev., 30, 47–62, 2011.
Liangcheng Tan, Yanjun Cai, Liang Yi, Zhisheng An, and Li Ai: Precipitation variations of Longxi, northeast margin of Tibetan Plateau since AD 960 and their relationship with solar activity, Clim. Past, 4, 19–28, doi:10.5194/cp-4-19-2008, 2008.
Tan, M., Liu, T. S., Hou, J. Z., Qin, X. G., Zhang, H. C., and Li, T. Y.: Cyclic rapid warming on centennial-scale revealed by a 2650-yr stalagmite record of warm season temperature, Geophys. Res. Lett., 30, 191–194, 2003.
Tan, M., Baker, A., Genty, D., Smith, C., Esper, J., and Cai, B. G.: Applications of stalagmite laminae to paleoclimate reconstructions: Comparison with dendrochronology/climatology, Quaternary Sci. Rev., 25, 2103–2117, 2006.
Tao, S. Y. and Chen, L. X.: A review of recent research on the East Asina summer monsoon in China, in: Monsoon Meteorology, edited by: Chang, C. P. and Krishnamurti, T. N., Oxford University Press, 60–92, 1987.
Thompson, L. G., Yao, T., Mosley-Thompson, E., Davis, M. E., Henderson, K. A., and Lin, P. N.: A high-resolution millennial record of the South Asian monsoon from Himalayan ice cores, Science, 289, 1916–1919, 2000.
Verschuren, D., Laird, K. R., and Cumming, B. F.: Rainfall and drought in equatorial east Africa during the past 1100 yr, Nature, 403, 410–414, 2000.
Wang, Y. J., Cheng, H., Edwards, R. L., An, Z. S., Wu, J. Y., Shen, C. C., and Dorale, J. A.: A high-resolution absolute-dated late Pleistocene monsoon record from Hulu Cave, China, Science, 294, 2345–2348, 2001.

CPD
8, 1275–1300, 2012

Wang, Y. J., Cheng, H., Edwards, R. L., He, Y. Q., Kong, X. G., An, Z. S., Wu, J. Y., Kelly, M. J., Dykoski, C. A., and Li, X. D.: The Holocene Asian monsoon: links to solar changes and North Atlantic climate, Science, 308, 854–857, 2005.

Wang, Y. J., Cheng, H., Edwards, R. L., Kong, X. G., Shao, X. H., Chen, S. T., Wu, J. Y., Jiang, X. Y., Wang, X. F., and An, Z. S.: Millennial- and orbital-scale changes in the East Asian monsoon over the past 224 000 yr, Nature, 451, 1090–1093, 2008.

Yancheva, G., Nowaczyk, N. R., Mingram, J., Dulski, P., Schettler, G., Negendank, J. W., Liu, J. Q., Sigman, D. M., Peterson, L. C., and Haug, G. H.: Influence of the intertropical convergence zone on the East-Asian monsoon, Nature, 445, 74–77, 2007.

Yang, B., Braeuning, A., Yao, T. D., and Davis, M. E.: Correlation between the oxygen isotope record from Dasuopu ice core and the Asian Southwest Monsoon during the last millennium, Quaternary Sci. Rev., 26, 1810–1817, 2007.

Yi, L., Yu, H. J., Ge, J. Y., Lai, Z. P., Xu, X. Y., Qin, L., and Peng, S. Z.: Reconstruction of annual summer precipitation and temperature in north-central China since 1470 AD based on drought/flood index and tree-ring records, Climatic Change, 110, 469–498, doi:10.1007/s10584-011-0052-6, 2012.

Zhang, D. E., Li, H. C., Ku, T. L., and Lu, L. H.: On linking climate to Chinese dynastic change: spatial and temporal variations of monsoonal rain, Chin. Sci. Bull., 55, 77–83, 2010.

Zhang, P. Z., Cheng, H., Edwards, R. L., Chen, F. H., Wang, Y. J., Yang, X. L., Liu, J., Tan, M., Wang, X. F., Liu, J. H., An, C. L., Dai, Z. B., Zhou, J., Zhang, D. Z., Jia, J. H., Jin, L. Y., and Johnson, K. R.: A test of climate, sun, and culture relationships from an 1810-yr chinese cave record, Science, 322, 940–942, 2008.

Zhang, Q. Y.: The relationship between the east summer Asia monsoon and the india monsoon, in: East Asia Monsoon and Storm in China, edited by: Institute of Atmospheric Physics, Chinese Academy of Sciences, Meteorological Press, Beijing, 266–273, 1998.

Zhang, Q. Y. and Tao, S. Y.: East Asia tropical and subtropical monsoons in the summer and precipitation in Eastern China in wet season, J. Appl. Meteorol. Sci., 9(Suppl.), 16–23, 1998.

Zhang, R. H.: Relations of water vapor transport from Indian monsoon with that over East Asia and the summer rainfall in China, Adv. Atmos. Sci., 18, 1005–1017, 2001.

Zheng, J. Y., Wang, W. C., Ge, Q. S., Man, Z. M., and Zhang, P. Y.: Precipitation variability and extreme events in Eastern China during the past 1500 yr, Terr. Atmos. Ocean. Sci., 17, 579–592, 2006.

CPD
8, 1275–1300, 2012

Table 1. Uranium and thorium isotopic compositions and ^{230}Th ages for sample BD by ICP-MS. The corrected ages are indicated in bold.

Sample	^{238}U (ppb)	^{232}Th (ppt)	^{234}U (measured)	^{230}Th/^{238}U (activity)	^{230}Th/^{232}Th (atomic × 10^{-6})	Age (yr BP) (uncorrected)	Age (yr BP) (corrected)	Age (yr AD) (corrected)
BD-1 mm	9567 ± 16	1428 ± 29	49.5 ± 2	0.0022	246 ± 5	173 ± 2	**169 ± 3**	**1781 ± 3**
BD-16 mm	7890 ± 92	2060 ± 8	48 ± 7	0.0028	176 ± 3	231 ± 7	**224 ± 8**	**1726 ± 8**
BD-29 mm	6028 ± 8	3902 ± 78	51.9 ± 2	0.0035	90 ± 2	308 ± 2	**290 ± 13**	**1660 ± 13**
BD-58 mm	7489 ± 57	2397 ± 8	42 ± 5	0.0061	313 ± 3	577 ± 8	**569 ± 9**	**1381 ± 9**
BD-75 mm	8925 ± 19	2518 ± 51	46.1 ± 2	0.0068	396 ± 8	647 ± 4	**639 ± 7**	**1311 ± 7**
BD-95 mm	7550 ± 12	1873 ± 38	49.8 ± 2	0.0073	488 ± 10	706 ± 3	**699 ± 6**	**1251 ± 6**
BD-106 mm	8713 ± 21	4296 ± 87	43.8 ± 2	0.0079	263 ± 5	764 ± 4	**750 ± 11**	**1200 ± 11**
BD-126 mm	7398 ± 55	2517 ± 8	41 ± 5	0.0093	450 ± 3	918 ± 11	**909 ± 12**	**1041 ± 12**
BD-148 mm	8891 ± 23	4702 ± 95	42.1 ± 2	0.0098	307 ± 6	973 ± 5	**958 ± 12**	**992 ± 12**
BD-192 mm	7943 ± 12	2260 ± 45	48.6 ± 2	0.0105	607 ± 12	1035 ± 3	**1027 ± 7**	**923 ± 7**
BD-207 mm	7444 ± 12	7468 ± 150	49.9 ± 2	0.0113	185 ± 4	1118 ± 20	**1090 ± 20**	**860 ± 20**

Errors are 2σ analytical errors. Decay constant values are $\lambda_{230} = 9.1577 \times 10^{-6}\,yr^{-1}$, $\lambda_{234} = 2.8263 \times 10^{-6}\,yr^{-1}$, $\lambda_{238} = 1.55125 \times 10^{-10}\,yr^{-1}$. Corrected ^{230}Th ages assume an initial ^{230}Th/^{232}Th atomic ratio of $(4.4 \pm 2.2) \times 10^{-6}$. Year BP: year before present (1950 AD).

CPD
8, 1275–1300, 2012

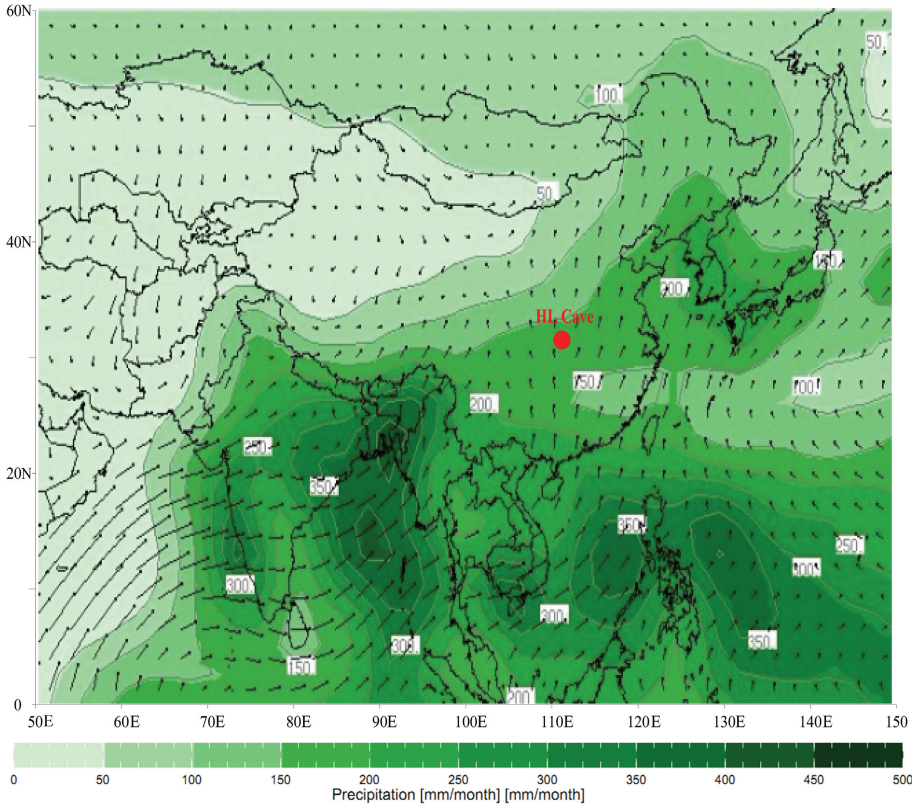

Fig. 1. Global mean July precipitation (mm month^{-1}) within the longitudinal and latitudinal ranges of 50° E–150° E, 0° N–60° N, including the site of Heilong Cave (HL, Central China, 31°40′ N, 110°26′ E, this study). Image from the website: http://iridl.ldeo.columbia.edu/. The numbers in the figure show the monthly rainfall. Climatological wind vectors for the 925 hPa pressure level indicate wind direction with speed proportional to the length of the vectors. The data source is NCEP, Climate Prediction Center USA.

CPD
8, 1275–1300, 2012

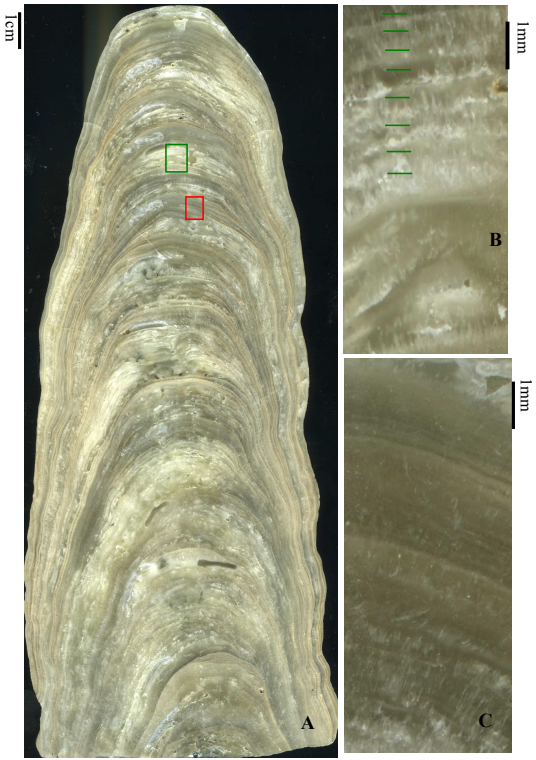

Fig. 2. (A) polished surface of sample BD, showing lamination alternations of white-porous and dark-compact calcite. **(B)** A higher magnification view of the area in the green rectangle in **(A)**, displaying annual layers in white-porous calcite. **(C)** A higher-magnification view of the area in the red rectangle in **(A)**, showing the examples of annual layers preserved in dark-compact lamination.

CPD
8, 1275–1300, 2012

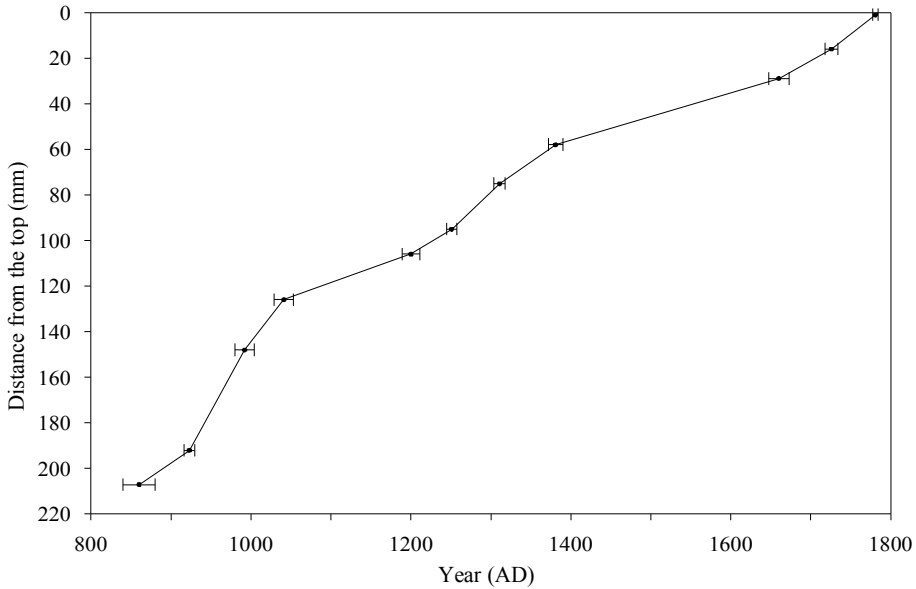

Fig. 3. A ^{230}Th age model for the stalagmite BD. Black dots with error bars depict ^{230}Th dates with age errors less than 20 yr (Table 1). The chronology was constructed by linear interpolation between ^{230}Th dates.

CPD
8, 1275–1300, 2012

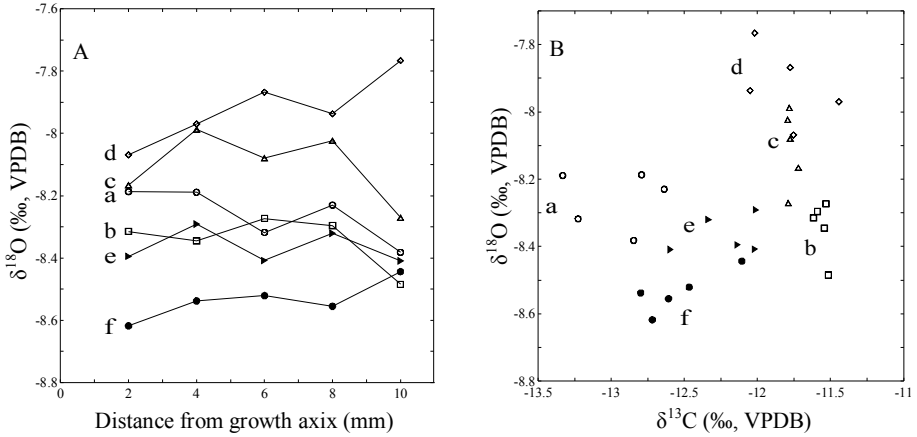

Fig. 4. The Hendy Test for the stalagmite BD. **(A)** δ^{18}O profiles along six growth layers (a to f) show no substantial isotopic fractionation. δ^{18}O variations along the same layer are relatively small (<0.3‰) compared with the variations along the growth axis. **(B)** δ^{18}O versus δ^{13}C for growth layers a to f. Correlations between δ^{18}O and δ^{13}C are statistically insignificant.

CPD
8, 1275–1300, 2012

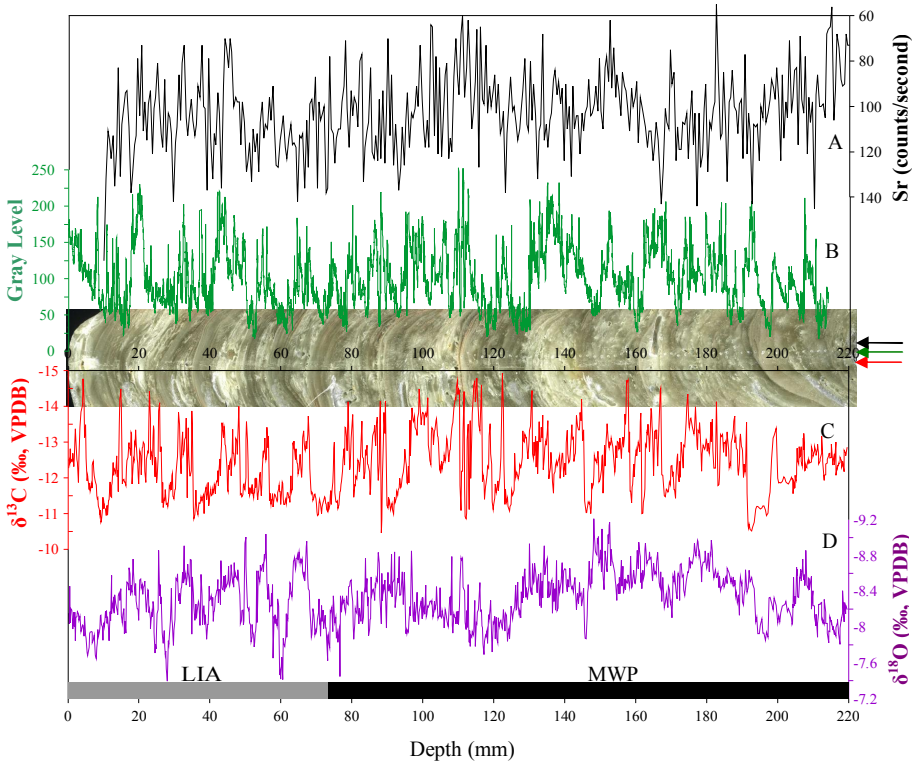

Fig. 5. Comparison between lithologic changes and multi-proxy records of stalagmite BD. **(A)** Sr record (counts/s, black curve); **(B)** Gray level record (green curve); **(C)** δ^{13}C record (red curve); **(D)** δ^{18}O record (purple curve). The sample photo is shown in the center for comparison. The black, green and red arrows indicate the analysis tracks of Sr, gray level and stable isotope, respectively.

CPD
8, 1275–1300, 2012

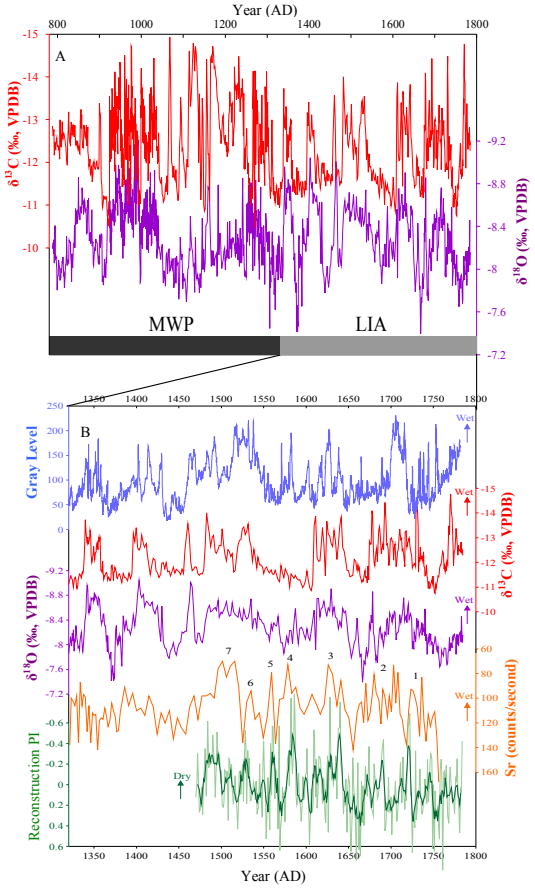

Fig. 6. (A) the $\delta^{18}O$ (purple curve) and $\delta^{13}C$ (red curve) time series. **(B)** detailed comparison of multi-proxy records from stalagmite BD and reconstruction precipitation index (PI) from Northern China (Yi et al., 2012), deep green line is 5-point running mean. The numbers indicate wet periods at the cave site over the mid-low Yangtze River Valley.

CPD
8, 1275–1300, 2012

Isotopic and lithologic variations of precisely dated stalagmite

Y. F. Cui et al.

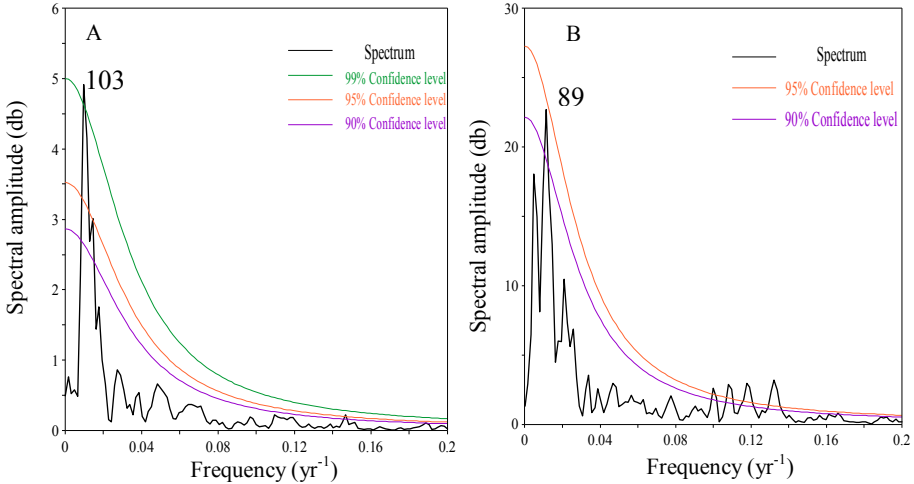

Fig. 7. Spectral analyses of the δ^{18}O **(A)** and δ^{13}C **(B)** records during LIA. Spectral peaks are labeled with their period (in yr). The spectra were calculated with software REDFIT (Schulz and Mudelsee, 2002).

CPD
8, 1275–1300, 2012